

DCO: Dynamic Cache Orchestration for LLM Accelerators through Predictive Management

Zhongchun Zhou , Chengtao Lai , Yuhang Gu , and Wei Zhang , *Fellow, IEEE*

Abstract—The rapid adoption of large language models (LLMs) is pushing AI accelerators toward increasingly powerful and specialized designs. Instead of further complicating software development with deeply hierarchical scratchpad memories (SPMs) and their asynchronous management, we investigate the opposite point of the design spectrum: a multi-core AI accelerator equipped with a shared system-level cache and application-aware management policies, which keeps the programming effort modest. Our approach exploits dataflow information available in the software stack to guide cache replacement (including dead-block prediction), in concert with bypass decisions and mechanisms that alleviate cache thrashing.

We assess the proposal using a cycle-accurate simulator and observe substantial performance gains (up to 1.80x speedup) compared with conventional cache architectures. In addition, we build and validate an analytical model that takes into account the actual overlapping behaviors to extend the measurement results of our policies to real-world larger-scale workloads. Experiment results show that when functioning together, our bypassing and thrashing mitigation strategies can handle scenarios both with and without inter-core data sharing and achieve remarkable speedups.

Finally, we implement the design in RTL and the area of our design is 0.064mm² with 15nm process, which can run at 2 GHz clock frequency. Our findings explore the potential of the shared cache design to assist the development of future AI accelerator systems.

Index Terms—Large Language Model, AI Accelerator, Analytical Model, Memory Management.

I. INTRODUCTION

WITH the advent of the artificial intelligence (AI) era, the demand for AI-tailored hardware has surged across various environments, from data centers to embedded systems. Since 2014, extensive efforts in academia and industry have led to the development of deep learning accelerator prototypes

A preliminary version of this paper appeared in the proceedings of ICS 2024.

Z. Zhou and C. Lai contributed equally to this work.

Z. Zhou and C. Lai are with the Department of Electronic and Computer Engineering, The Hong Kong University of Science and Technology, Clear Water Bay, Kowloon, Hong Kong (e-mail: zzhouch@connect.ust.hk; claiac@connect.ust.hk).

Y. Gu is with the School of Electronic Science and Engineering, Southeast University, Nanjing, Jiangsu, China

W. Zhang (corresponding author) is with the Department of Electronic and Computer Engineering, The Hong Kong University of Science and Technology, Clear Water Bay, Kowloon, Hong Kong (e-mail: eeweiz@ust.hk).

© 2025 IEEE. Personal use of this material is permitted. Permission from IEEE must be obtained for all other uses, in any current or future media, including reprinting/republishing this material for advertising or promotional purposes, creating new collective works, for resale or redistribution to servers or lists, or reuse of any copyrighted component of this work in other works.

and chips, such as Eyeriss [5], Gemmini [13], and industry examples like Google’s TPUs [17], [18], and Huawei’s Ascend 310 and 910 [28]. These accelerators span a broad spectrum, from power-efficient devices to those designed for high computational throughput [34].

AI accelerators, compared with Graphics Processing Units (GPUs), can be optimized for AI applications and tailored for specific scenarios, such as pre-defined neural network (NN) computation graphs, operator types, certain data precision, and given power budgets. Since they are often used in scenarios where the execution graph is known during compilation, they typically employ software-controlled scratchpad memories (SPMs) as the on-chip storage. SPMs, similar to caches, are also Static Random-Access Memories (SRAMs), but lack address tags and status bits. This design choice undoubtedly simplifies hardware design, leaves more chip area for computing units and on-chip storage, and enables higher performance due to asynchrony. However, these benefits also come with costs. In addition to SPM data fragmentation that needs to be resolved during graph compilation [30], data transfer between SPMs and the main memory needs to be scheduled explicitly by programmers or compilers. Such transfer primitives are often designed to be asynchronous to enable computation-communication overlap, so barriers are also required. Simple as they seem, programming will quickly become prohibitive when combined with some other features: (1) when multiple levels of on-chip buffers exist (e.g., Cambricon’s BANG-C programming model requires a 5-level pipeline and > 200 lines of code only to implement a high-performance vector add [4]), (2) when the programming model is SIMD-based (Single Instruction Multiple Data) which requires handling unaligned cases and tail blocks carefully. Hence, **to alleviate these management difficulties**, our work explores the potential of a **hybrid architecture that replaces shared SPM hierarchy with a last-level cache (LLC)** in AI accelerators.

This choice is not uncommon, as is demonstrated by the extensive use of NVIDIA GPUs in AI workloads. However, the impact of caches on large-scale AI accelerator systems remains underexplored. In this work, we examine the role and strategies of cache management in the context of deep learning and LLMs. Our contributions include:

- We propose a novel “Tensor Management Unit” (TMU) that is integrated into the memory hierarchy to aid cache management. We implement our design using Chisel HDL [2] and synthesize the design with a 15nm process library for practical evaluation.

- Based on metadata stored in TMU, we design a self-adaptive anti-thrashing mechanism, a dead-block prediction scheme, and a dynamic bypassing policy that work cooperatively to help the cache capture reuses within a large working set.
- We establish an analytical model through bottleneck and overlapping analysis, and have validated it against our cycle-level simulator. This enables us to evaluate our strategies under real-world larger-scale cases.

II. BACKGROUND AND MOTIVATION

Below, we first briefly review the basics of Transformers and FlashAttention, which then lead to a short discussion on existing GPU/AI accelerator architectures and their limitations. After that we show the factors that motivate us to incorporate a system-level cache instead of an SPM in AI accelerators, as well as how our proposal aligns with current trends: (1) (explained in Section I) shared SPM management becomes increasingly complex in conventional architecture, while using a shared cache can ease development; (2) System-on-Chips (SoCs) in cell phones and autonomous vehicles usually involve a system-level cache, so we also try gaining insights on using it for LLMs without introducing additional large buffers; (3) Our work is an example of exposing tensor-level information to the hardware, a trend already present in current GPUs.

A. Transformer and Large Language Model

Large Language Models (LLMs) have become prevalent in recent years, and transformer-based units are the kernel behind them. Despite the similarities between LLMs and conventional DNNs, their different network topologies, tensor shapes and application scenarios have brought about brand-new computation features and challenges in AI accelerator designs. Previous works [19], [24] have revealed the intense memory boundness in activation-activation multiplication, as opposed to conventional CONV and FC operators. They have also pointed out that the quadratic growth of intermediate tensor size (QK^T) with respect to sequence lengths, sometimes reaching tens of Gigabytes, makes on-chip data allocation and data reuse difficult [19].

B. FlashAttention

Due to the above reasons, self-attention normally features a low compute/memory access ratio, which means the computing units are often significantly underutilized. As a widely accepted solution, FlashAttention [9] leverages online softmax to store and update each attention score tile on-chip, hence eliminating the need to materialize it in the global memory.

As the GPU architecture evolves, FlashAttention has also experienced several major updates. FlashAttention-2 [8] reduces non-matmul OPs to better utilize the Tensor Cores, modifies the dataflow to better parallelize the thread blocks among SMs, and improves work partition between different warps of a thread block to reduce shared memory access. FlashAttention-3 further exploits features introduced in Hopper GPUs: asynchrony between Tensor Cores, CUDA Cores

and Tensor Memory Accelerator (TMA), and the more powerful low-precision computing capacity.

However, little effort has been made from a general architecture's perspective that does not require completely rewriting operator programs. TMA and warp specialization are unique to recent NVIDIA GPUs and may not see their counterparts in other GPUs or NPUs. Due to the deep software pipelines, FlashAttention-3 [36] can be register-bound on Hopper GPUs, but this may not be the case for other devices. In other words, the performance bottleneck shifts with system resources and the implementation of operators, and the latter further varies from device to device. To broaden the scope of this work, we only augment the shared cache with some universal strategies and do not make other specific architectural assumptions.

C. AI Accelerators in SoCs and Existing Architectural Support

We focus on multi-core accelerators with a shared last-level cache. Such designs are preferred over single-core embedded ones, such as Eyeriss-style chips [5], because LLM workloads are typically deployed on multi-core or multi-accelerator systems, and previous works have shown downgraded scalability through increasing computing and memory resources inside a single AI core in terms of performance and energy efficiency [12], [37].

An increasing number of commercial SoCs already integrate AI accelerators alongside CPUs and GPUs, and expose a shared system-level cache to all compute agents. Examples include mobile SoCs such as the Qualcomm Snapdragon X Elite series [6] and ARM's DynamicIQ-based designs [7], where a common LLC is used to reduce dark silicon and improve overall chip efficiency. In such systems, the system-level cache is effectively irreplaceable by a private scratchpad, because it also serves CPUs and other agents. This makes "how to use an existing shared cache for AI/LLM workloads" a more realistic question than "whether to add a new large global buffer".

In addition to a shared cache, recent industrial designs have begun to move structured tensor metadata closer to the hardware. For instance, NVIDIA's Hopper architecture introduces TMA engines and tensor maps that encode multi-dimensional addresses, strides, and layouts; these descriptors are consumed by specialized load instructions to orchestrate asynchronous tile transfers into shared memory for kernels such as FlashAttention. Similarly, Triton-based kernels organize tensor accesses around lightweight descriptor objects (i.e., `triton.language.make_tensor_descriptor`), which capture base pointers, shapes, and strides and are used to generate TMA instructions.

These mechanisms show that exposing tensor-level information (shape, layout, tiling) to the hardware is already a widely adopted practice in high-performance LLM implementations. However, such metadata is typically confined to driving local SRAM transfers and kernel-specific software pipelines, failing to systematically coordinate the behavior of a shared last-level cache across multiple cores.

Our work can be viewed as generalizing this trend from per-kernel tensor descriptors to a reusable architectural primitive

for shared-cache management. Instead of embedding tensor metadata only inside individual kernels, we introduce a small Tensor Management Unit that maintains per-tensor and per-tile information and feeds it to the LLC replacement and bypass logic. This allows the shared cache to make predictive decisions—such as dead-block identification, anti-thrashing prioritization, and dynamic bypassing—based on the same type of high-level tensor descriptors that are already common in modern LLM software stacks.

In summary, existing SoCs increasingly provide a shared system-level cache that is already on the critical path of AI/LLM workloads, and industrial software/hardware stacks have begun to expose rich tensor descriptors to drive fine-grained data movement. Building on these trends, our work studies how to orchestrate a shared LLC among multiple AI cores using lightweight tensor-level metadata, rather than relying solely on software-managed SPMs. We do not assume any specific AI core microarchitecture; instead, our DCO mechanisms only require that cores issue bulk transfers between their private SPMs and the shared cache, making the proposed techniques applicable to a wide range of GPU- and NPU-like systems.

III. SYSTEM ARCHITECTURE OVERVIEW

A. Baseline SoC Integration Options

The integration of AI accelerator into the whole SoC becomes a common practice, but the architectural designs and the mechanism of data sharing between CPU and AI accelerator vary. Previous works typically assume an SoC configuration like Figure 1(b)-(d). (b) and (c) are solely SPM-based. (d) guides the traffic from accelerators to the CPU L2 cache, relieving the compiler from shared SPM allocation, while still capturing data reuse between AI cores. Despite the existence of alternative methods proposed in works such as [10] to mitigate the impact of substantial accelerator traffic on CPU execution, the inherent CPU-NPU intervention remains a persistent challenge. The existence of cache pollution makes the performance change increasingly unpredictable and unexplainable when altering the internal mechanism and replacement policies of the shared cache.

B. Proposed DCO-Based SoC Architecture

To mitigate cache pollution imposed by CPUs, we adopt the configuration depicted in Figure 1(e). This architecture retains the advantage of Figure 1(d): no need for shared buffer allocation and thus more friendly to the compiler.

Note (e) is an architectural abstraction where CPU and accelerator traffic are separated. For a real SoC, the logical behavior can approximate either (d) or (e) depending on whether CPU traffic is configured to bypass the accelerator-shared cache. This shared cache architecture among AI cores resembles that of a GPU, where each core with its private SPM corresponds to a stream multiprocessor (SM).

C. Architectural Challenges for Multi-core AI Systems

Despite this architectural similarity, shared cache utilization in our system differs from that in a GPU since GPUs

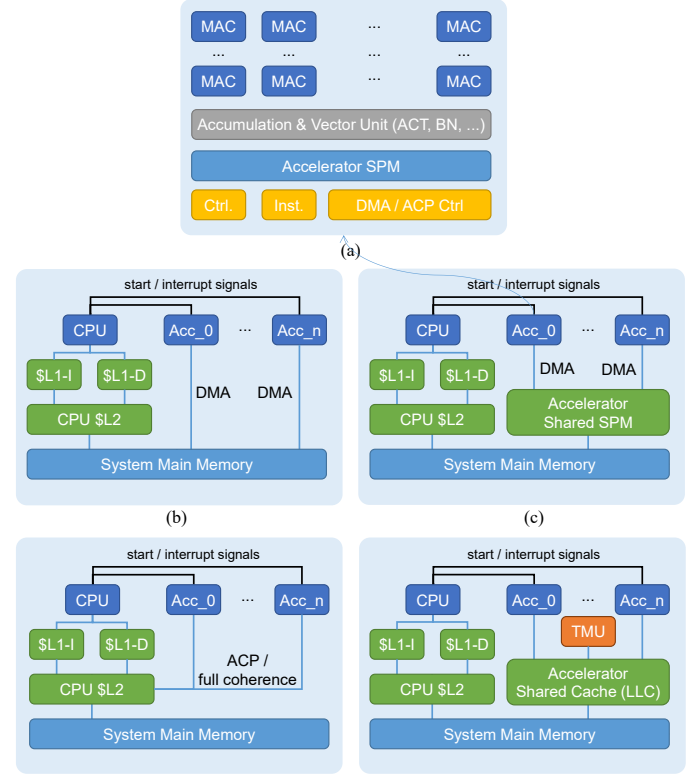


Fig. 1. (a) A typical AI accelerator structure. (b) SoC with accelerators directly connected to DRAM via DMA. (c) SoC with accelerator cores connected to a shared SPM. (d) SoC with accelerator cores connected to the CPU L2 cache. (e) (ours) SoC with accelerator cores first connected to a shared cache (assisted by an additional “TMU”).

have inherent mechanisms of context switch to hide memory latency, while AI accelerators rely on explicit scheduling of bulk data transfers. In systems with shared SPMs, latencies of memory transfer are rather predictable with hardware parameters. However, in cache-based systems, latencies will change dramatically on cache hits and misses. Furthermore, Transformer and FlashAttention kernels would put the shared cache under stress, because the working set for long-context LLMs could far exceed the LLC capacity. Naive Least Recently Used (LRU) replacement will degenerate into thrashing: useful lines are frequently evicted before their next use, so the hit rate becomes remarkably low or even 0, nearly independent of the cache size. The observation thus motivates us to design a replacement and bypass policy that can capture as much reuse as possible from an oversized working set.

D. Role of the Tensor Management Unit (TMU)

To address the above challenges, a replacement and bypass policy alone is not sufficient; it also needs high-level information about tensor lifetimes and dataflow that is typically only known to software. At the same time, only the hardware has real-time visibility into resource usage and cache pressure. With this in mind, we propose to provide the hardware with workload information that was originally only attainable from the software side. We aid the shared LLC with auxiliary data structures that hold information about the workload. We have also added additional hardware units to react in different situations with the help of such data structures. The additional unit (TMU) is shown in orange in Figure 1(e). The cache’s

TABLE I
VARIABLES USED IN THE PROPOSED ARCHITECTURE

Symbol	Meaning	Related Criteria
D_LSB	least significant bit to select bits from tag when looking up <code>dead_fifo</code>	consider as dead if <code>tag[D_MSB:D_LSB]</code> in <code>dead_fifo</code>
D_MSB	most significant bit to select bits from tag when looking up <code>dead_fifo</code>	bypass if <code>tag[B_BITS-1:0] < B_GEAR;</code>
B_BITS	bits to select from tag when deciding bypass; also used in anti-thrashing	anti-thrash: first evict lines with smaller <code>tag[B_BITS-1:0]</code>
B_GEAR	threshold to determine whether to bypass a cache line	move a tile identifier from live tile info to dead tile identifiers if <code>accCnt == nAcc</code>
accCnt	number of accesses of a certain cache line, updated upon each access	
nAcc	expected number of accesses of each cache line of a tensor	

replacement and bypass logic then consults lightweight TMU-provided hints to implement dead block prediction (predicting cache lines that have finished their lifespans), anti-thrashing, and dynamic bypassing. The detailed microarchitecture and metadata formats are described in Section IV.

IV. MIXED-STRATEGY CACHE MANAGEMENT FOR DEEP LEARNING WORKLOADS

A. Dead Block Prediction and Anti-thrashing

As two perspectives to enhance performance, dead block prediction and anti-thrashing strategies have been widely discussed for conventional CPU architectures and workloads, but still require specialized solutions for AI accelerators running data-intensive workloads like Transformers.

Replacement policies (RPs) like LRU generate victims according to the access history. But the ranks of cache lines given by such RPs do not necessarily reflect their life cycles. Fortunately, for a given dataflow, the number of reuses can be precisely known before computation (e.g., Figure 2(a)), making a counter-based method feasible.

At the high level, we integrate our solution into the RP. When searching for a victim, it first tries to find a dead block. If no dead block is found, it turns to the anti-thrashing policy, which keeps a certain subset of the working set in the cache. If this procedure produces a tie, it falls back to LRU to select the final victim within those anti-thrashing candidates. Straightforward as it is, the hardware should be implemented with special optimizations to reduce area and latency overhead.

B. Hardware for Dead Block Prediction and Anti-thrashing

Section IV-A demonstrates the necessity of using dataflow-related information of cache lines for a better replacement policy. In our design, this is achieved by introducing an additional hardware unit named tensor management unit (TMU). TMU acts as a liaison between software and hardware: metadata of tensors and tiles are written into TMU by the CPU after allocation and before operator computation, so dynamic shapes are also supported; the metadata are later retrieved by the replacement policy to get the victims. These metadata are managed at a **tensor- and tile-level instead of a cache-line level** since cache lines in the same tile share the same properties. A coarser granularity also reduces resource usage since it requires fewer entries. Configuration parameters involved in TMU are listed in Table I, and will be explained when they are first referenced.

Figure 2 (b) shows the internal structure of TMU and how it interacts with the rest of the system. TMU is made up of two components: the tensor metadata module and the tile

metadata module. The former keeps static operator metadata that are registered before execution, while the latter consists of live tile info and dead tile identifiers, both of which assist cache replacement and are updated during runtime using tensor metadata. `accCnt` in the live tile info module will be updated when the tile's last cache line (TLL) is accessed. Three specialized instructions are designed for the CPU to register dataflow-related information into the TMU:

- Tensor metadata: Expected `numAccess` (determined by dataflow, a.k.a. `nAcc`), tensor base address, whether to bypass the whole tensor from LLC, tile size of the tensor, and operand id (e.g, left operand / right / output);
- Clear: Clear the current registration if no longer needed;
- Set other parameters: `D_LSB`, `D_MSB`, `B_BITS`.

During accelerator computation, the TMU functions as follows:

- When an AI core requests an `addr`, the LLC informs TMU of this access. If it is a TLL, `accCnt` increases by 1. If it reaches the expected `nAcc`, the entry will retire from the live tile info module, and the bits `tag[D_MSB:D_LSB]` will be recorded into the dead tile identifier FIFO;
- The size of the dead tile identifier FIFO is designed to be limited to achieve a short access latency so that replacement decisions can be made within a clock cycle. When the FIFO is full, an old element will be cleared.
- When the replacement policy needs to select a victim, it queries the FIFO to judge whether the cache set contains a dead block. This information along with the anti-thrashing policy (Section IV-C) will be used for the cache replacement policy.

C. Self-adaptive Anti-thrashing

The anti-thrashing policy prioritizes part of the cache lines while sacrificing the others. Rather than manually tune the management parameters according to cache size by engineers, we design a scheme with a self-adaptive nature.

We crop a segment in the cache tag, `tag[B_BITS-1:0]`, to decide the relative priorities of cache lines. These are the lowermost bits of the tag domain, so we expect this value to span a uniform distribution across a tensor. We let the replacement policy evict cache lines with smaller `tag[B_BITS-1:0]` values first. If the result produces a tie, it will use the default LRU result. The smaller the cache is, the fewer cache lines it will keep, and the more it will sacrifice to mitigate thrashing.

To accommodate varying requirements in diverse applications, we can use different `B_BITS` values. A larger `B_BITS`

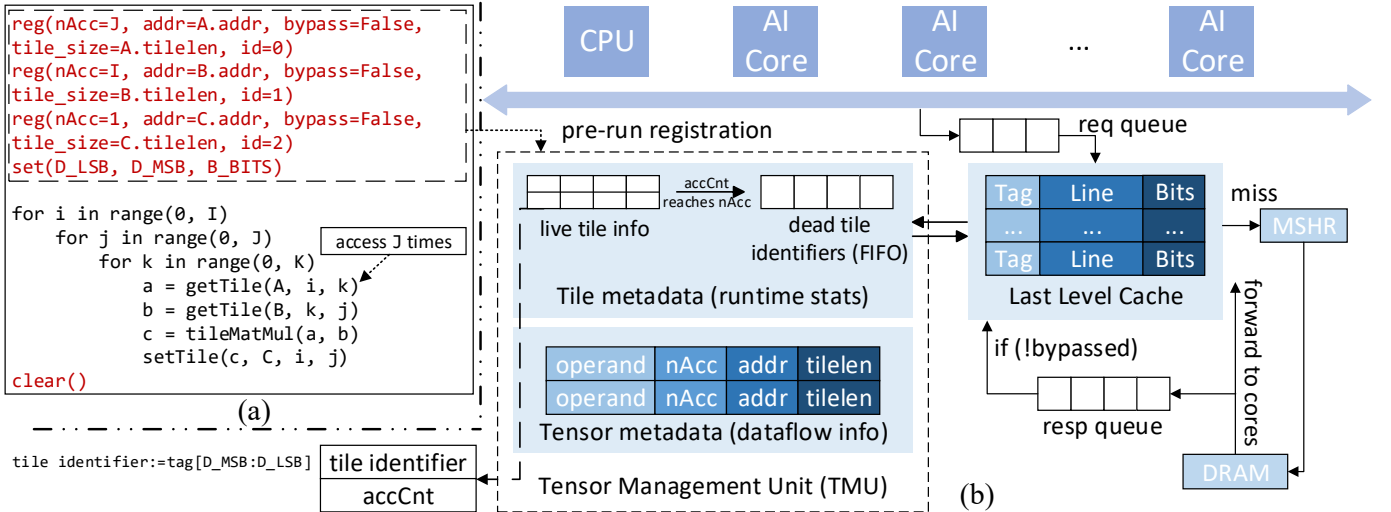


Fig. 2. (a) Pseudo code of tiled MatMul. nAcc: expected number of accesses of each tile in this matrix; getTile: load the tile into the AI core private SPM; setTile: store the tile into the memory system from the AI core private SPM. Lines in red are manually-inserted registration codes to pass dataflow-related information to TMU. (b) System architecture and workflow with TMU. The interaction between LLC and TMU is elaborated in Section IV-B.

means a finer control over cache thrashing but also leaves smaller space for LRU, and vice versa. The detailed experiments and analysis are in Section VI-D3.

D. Coordinated Dynamic Bypassing

Even a well-structured replacement policy, as described in Section IV-B and IV-C, can be overwhelmed when the working set is significantly larger than the cache. To further mitigate this, we augment the anti-thrashing mechanism with a dynamic bypassing policy that works collaboratively. The connection between them is a unified priority scheme, i.e., using the same least significant bits of an address tag as a priority score ($t_{tag[B_BITS-1:0]}$) to control their decisions.

- **Replacement Policy:** During an eviction, the anti-thrashing mechanism selects a victim from the lowest-priority tier currently present in the cache set. This approach protects higher-priority data, helping to maintain a smaller working set under pressure.
- **Bypass Policy:** Upon a cache miss, if the incoming data has a low priority score, it may be a candidate to bypass LLC. This preemptive action spares the cache from allocating space for data that would likely be a primary eviction candidate anyway.

This synergy is crucial to avoid conflicts between anti-thrashing and bypassing. By steering low-priority traffic away from the cache with the same criterion, the design further sidesteps the problem of cache pollution and thrashing.

Similar to anti-thrashing, our bypassing policy can also adapt itself to the varying memory pressure at runtime. This is achieved via a runtime-adaptive threshold B_GEAR , which is managed independently among different cache slices. This gear determines how many of the lowest-priority tiers are subject to bypassing. The system dynamically tunes this value based on observed cache contention, measured via the LLC eviction rate over a sliding window, i.e. how many cache evictions in a certain slice during a recent time frame. This feedback loop operates as follows:

- If the eviction rate surpasses a threshold ($bypass_ub$), it signals severe cache thrashing. The system responds by increasing B_GEAR , thereby bypassing more low-priority data to alleviate pressure.
- Conversely, if the eviction rate falls below a threshold ($bypass_lb$), it indicates that the cache has ample capacity. The system then decreases B_GEAR , allowing more data to be cached to maximize the potential hit rate.

This adaptive behavior allows the system to subtly flip its strategy: from maximizing hit rates when contention is low to aggressively pruning pollution as pressure mounts. This interplay between the replacement policy, bypassing, and runtime adaptation enables the significant performance gains observed in our at+bypass and at policies in Figure 4.

E. A Variant of Bypassing in Inter-core Sharing Cases

Bypassing and anti-thrashing are both designed to mitigate cache contention, but they have different capacities to handle inter-core sharing scenarios, e.g., when the workload feature a spatial group allocation dataflow (Section VI-C). In an LRU cache, even if inter-core reuses are not merged in the MSHR, the cache storage can hold the data for a while, so these reuses are still likely cache hits. This property also holds true for anti-thrashing, as deprioritized data also stay in the cache for a while before getting evicted; but if some of these addresses are bypassed upon the first access, additional memory fetches will be required, taking up more memory bandwidth and leading to even poorer performance than LRU. In other words, **bypassing blindly will miss some inter-core reuse opportunities**.

Therefore a more conservative bypassing variant, which we term `gqa_bypass`, is preferred in such cases to avoid excessive memory traffic. In our experiments, we only bypass data fetched by the slower core in a core pair (i.e. the core that commits fewer instructions) when the LLC is highly contended, while data fetched by the faster core is always cached. This strategy, along with the anti-thrashing policy, strikes a balance between reducing cache contention and avoiding excessive memory accesses.

V. CACHE-INTEGRATED ANALYTICAL MODEL FOR AI ACCELERATORS

A. Cycle-level Simulator and Analytical Model

Despite the relatively accurate results offered by cycle-level simulators, their long running time significantly confines the simulated workload size. In addition, large models exhibit distinct computational characteristics that cannot be simply scaled up and deduced from the results of smaller models. A typical factor is the warm-up period of each simulation. We also empirically confirmed that directly scaling up the running time of small cases to larger ones results in unstable variations. Hence, in addition to evaluating our design with a cycle-level simulator, we have built an analytical model to extend its measurement results to real-world cases. It does not need to precisely model every variant of our policies; it is acceptable as long as it provides a proxy or a bound to a properly-set policy. For instance, below we only model the optimal static bypassing that should be the upper limit of our dynamic bypassing policy.

B. Overlapping Mechanism

In a GPU-like architecture, a key factor that determines performance is how memory access time is hidden by computation. A conventional perspective is that GPUs can switch to other warps when one warp is blocked by ongoing memory requests. But in FlashAttention, all warps start with a bulk transfer from the global memory to shared memory, followed by shared memory accesses and computation. These two steps would repeat several rounds, and finally a writeback is performed. Without explicit pipelining, it is likely that all thread blocks assigned to an SM are blocked by GDDR or HBM accesses, and thus cannot find computation instructions to hide latency, as is the case in FlashAttention-2. In other words, the overall time is not simply the maximum or the sum of memory transfer and computation time.

We model this behavior in our cycle-level simulator and try to understand the underlying overlapping mechanism. We notice that the **time consumed by a certain type of request is determined by its corresponding bottleneck**. For instance, cache hits and MSHR hits (memory requests merged into an existing MSHR entry) are bottlenecked by either the LLC bandwidth or the memory instruction issuing parallelism in the cores (bounded by load-store units). Similarly, MSHR misses are bottlenecked by the following with the lowest throughput: the cores, LLC, and main memory. Normally for a well-designed system, a hierarchy closer to the cores would have a higher throughput, but we still keep the max operators across all hierarchies in Eq.1 to ensure robustness in the design space.

Inspired by works on CPU analytical models [40], we divide cache misses into cold misses and conflict/capacity misses. Cold misses usually occur in a continuous manner, while the latter are more dispersed in the instruction flow. If conflict misses are sparse enough such that the LLC is not stalled, these misses are in fact “imperceptible” to the cores since they are not blocked by the downstream memory hierarchies. In other

words, conflict miss time can be hidden by computation, which translates to our final overlapping model in Eq.2.

$$\begin{aligned} t_{hit} &= \max \left\{ \frac{n_{hit}}{N \cdot ipc_{mem}}, \frac{n_{hit}}{v_{LLC}} \right\} \\ t_{cold} &= \max \left\{ \frac{n_{cold}}{N \cdot ipc_{mem}}, \frac{n_{cold}}{v_{LLC}}, \frac{n'_{cold}}{bw_{cold}} \right\} \\ t_{cf} &= \max \left\{ \frac{n_{cf}}{N \cdot ipc_{mem}}, \frac{n_{cf}}{v_{LLC}}, \frac{n'_{cf}}{bw_{cf}} \right\} \end{aligned} \quad (1)$$

$$t = t_{hit} + t_{cold} + \max\{t_{comp}, t_{cf}\} \quad (2)$$

Variables starting with t and n are the time (clock cycles) consumed by a type of request and its total number across all cores, while subscripts cf , hit , $cold$ and $comp$ stand for conflict/capacity misses, MSHR and cache hits, cold misses and computation plus local scratchpad access. N is the number of cores. n' means the number of requests sent to the main memory after being merged by the MSHR. ipc_{mem} represents the maximum possible number of global memory \leftrightarrow local scratchpad transfer instructions issued each cycle in each core (similar for ipc_{comp}); v_{LLC} is the throughput of the LLC; bw is the actual main memory bandwidth (all counted in number of requests per cycle). Also note $t_{comp} = n_{comp}/(N \cdot ipc_{comp})$. n_{comp} and n_{cold} can both be derived from dataflow information.

C. Estimating Cache and MSHR Hits

In our dataflow assumption, each dimension can be tiled in either the spatial or temporal domain. In GQA FlashAttention operators, if the Group dimension is (at least partially) mapped to multiple cores (i.e., spatial group allocation in Section VI-C), KV tensors will be shared among cores. This inter-core data reuse can be captured by either the MSHR or LLC: If these memory requests reach LLC closely enough, they are likely to be merged by the MSHR; otherwise, these MSHR merging events will be converted into cache hits, if they are not yet evicted. As the LLC is highly pipelined, MSHR hits and cache hits can be handled at the same throughput (v_{LLC}). Thus, without loss of generality, the time consumption of such inter-core reuses can be calculated by combining the reuses captured by LLC and its MSHR in a single term.

Now let us consider the effect of temporal reuses. For generic workloads, CPU analytical models like SDCM [3] have already proposed a mature model to predict hit rates with a given reuse distance profile. As our workload features streaming through K/V tensors repeatedly (Query and Output tensors are always bypassed from LLC as their tiles are held in the local SPM until the end of life cycle and they are fetched from DRAM only once), the hit rate for an LRU cache is simply 100% when the reuse distance (uniform across K/V elements) is no larger than the cache size and 0 otherwise. Our bypassing and anti-thrashing strategies attempt to make use of LLC in the latter scenario by keeping only a subset of K and V. For ideal bypassing, this subset size should be exactly the cache size. Our self-adaptive anti-thrashing strategy is equivalent to calculating such S_{kept} and the maximum possible

integer M that $S_{kept} = S_{work} \cdot M / 2^{B_BITS} \leq S_{LLC} \cdot (A-1)/A$, where S_{kept} , S_{work} and S_{LLC} correspond to the size of the prioritized subset, the working set, and LLC, respectively, while A denotes associativity. Reuses of the kept subset are thus counted into n_{hit} . The term $(A-1)/A$ means at least one cache line per set is used to temporarily place new lines. By far, for a given dataflow, all n and n' in Eq.1&2 can be calculated for LRU, anti-thrashing, and ideal bypassing.

D. Estimating Bandwidth Utilization

Our experiments reveal that cold misses usually occur in bursts, so they can saturate the main memory bandwidth. Conflict and capacity misses are more dispersed in the instruction flow, so their bandwidth utilization should be calculated based on the rate of demand $v_{cf,dmd}$, which depends on n_{cf} , v_{LLC} , and the density of conflict miss instructions η_{cf} :

$$v_{cf,dmd} = \min \{ \eta_{cf} N \cdot ipc_{mem}, v_{LLC} \}$$

$$\eta_{cf} = \frac{n_{cf}/ipc_{mem}}{n_{mem}/ipc_{mem} + n_{comp}/ipc_{comp}} \quad (3)$$

where $n_{mem} = n_{hit} + n_{cold} + n_{cf}$ is the total number of memory transfer instructions of all cores and can be calculated directly from dataflow information. As for the actual bandwidth utilization bw_{cold} and bw_{cf} , we empirically find

$$bw_{cold} \approx \theta_1 BW \quad (4)$$

$$bw_{cf} \approx \text{clip}(\lambda v_{cf,dmd}, \theta_2 BW, \theta_3 BW) \quad (5)$$

where BW is the theoretical memory bandwidth calculated from the DRAM specifications, while $\theta_1, \theta_2, \theta_3$ ($\theta_2 < \theta_3$), λ are constant coefficients for a given combination of ipc_{mem} , main memory, LLC bypass and replacement policy.

E. Other Assumptions and Discussions

Our analytical model does not model the effect of instruction window size, since this should not be a major bottleneck for a well-designed architecture. In our simulation, this size is selected such that it makes almost no difference from the performance of an infinite instruction window while still in a reasonable range. We also realize that DRAM access pattern is one of the major factors that determine bandwidth utilization (i.e., $\theta_1, \theta_2, \theta_3$). We try to capture the main trend across hardware configurations and control the error to a reasonable limit, as predicting minor fluctuations is beyond the scope of an analytical model.

In addition, recent GPUs/NPUs differ not only in their ratio of computing and memory access resources but also in several key mechanisms. The former can be modeled with different values of n_{comp} and ipc_{comp} . Mechanisms like warp specialization and TMA in Hopper GPUs even allow t_{cold} to partially overlap with t_{comp} , but we believe our philosophy of bottleneck analysis is applicable to all such devices.

VI. EXPERIMENTS AND RESULTS

A. Cost Evaluation

Our design is implemented in Chisel HDL and synthesized by Synopsys Design Compiler with a 15nm open-source

library NanGate 15nm OCL [31]. The synthesis results are shown in Table II, using the system configuration parameters in Table III.

TABLE II
HARDWARE SYNTHESIS RESULTS

Module	Max frequency	Area
TMU	2.0 GHz	64,438 (μm^2)

TABLE III
HARDWARE CONFIGURATIONS

Variable	Settings
LLC Slice	32
Physical Address Width	48-bit
Tensor Metadata Entry Number	8
Tile Metadata Entry Number	256
Dead FIFO Depth	16

B. Simulation Infrastructure and Hardware Configuration

Our strategies influence the behaviors of the memory subsystem, so a cycle-level simulator is needed for evaluation. However, current simulators fail to meet our demand for the following reasons. (1) Most of the open-source AI accelerator simulators do not support a shared last-level cache; (2) Existing ones like SMAUG [42] are too slow since they involve too many details of in-core datapaths, which are unnecessary when our major concern is the LLC; (3) GPU simulators like Accel-Sim [21] deeply embed GPU-specific assumptions into their code (e.g., fixed warp sizes, complex warp scheduling mechanism, running on real PTX code). These details severely confine the generality of our design and hinder efficient dataflow exploration since rewriting these kernels with manual effort is far more time-consuming and error-prone compared to directly using memory traces generated from given dataflows.

Considering the above requirements and constraints, we adopt the cycle-level simulator proposed in LLAMCAT [45], which is specifically designed for LLM workloads with flexible memory-hierarchy modeling. The simulation configurations are detailed in Table IV. This simulator supports shared LLC, trace-driven evaluation, and configurable dataflows, making it well-suited for the studies in this paper.

However, this simulator will still be overwhelmed when running operators from real-world LLMs. For these large-scale workloads, we have fitted an analytical model (Section V) and validated it against cycle-level simulation results. In the following sections involving cycle-level simulation, cache sizes are set to be relatively small to expose this bottleneck; they will be set to more realistic values when we scale up the problem to real-world sizes.

C. Workloads

We use Gemma3-27B, Llama3-70B, Llama3-405B, and Qwen3-8B as benchmarks throughout this section. In each attention unit, these models mainly differ in the number of Q

TABLE IV
SIMULATED SYSTEM CONFIGURATIONS

Basics	frequency=2.0GHz, 16 cores, 1MB-16MB LLC, 32 LLC slices
Core	inst_window_depth=128, num_inst_windows=1 1 core=1 vector unit + private Scratchpad Memory, vector-len=128B
LLC slice	associativity=8, data-latency=25, num-target=8, mshr-num-entry=6 (per slice), alloc-on-fill, write-back, write-allocate, resp_q_size=64, req_q_size=12
LLC req-req arbitration	response-queue-first
DRAM	DDR5_8Gb_x16, DDR5-3200, 4 ranks, 16 channels

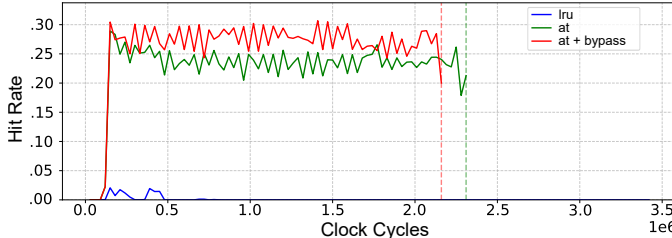


Fig. 3. Cache hit rate over time for LRU and our policies for a 4MB LLC (Gemma3-27B, 2K sequence length). The at policy demonstrates a consistently higher hit rate compared to LRU under contended conditions.

heads and KV heads. We focus on FlashAttention-2 in this paper since (1) we do not assume features like TMA and warp specialization, (2) it exhibits a more complex dataflow than GEMMs, and (3) GEMMs have been covered in the preliminary version of our paper [27]. In addition, these models all feature grouped-query attention (GQA): it lets a group of Q heads to share a single KV head to reduce KV cache size. As GQA introduces additional data sharing, it may perform differently compared to classical multi-head attention.

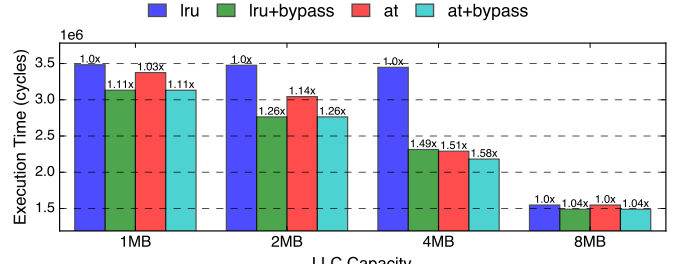
In addition, dataflows will directly influence reusing behaviors and thus overall performance. In GQA FlashAttention, one of the key factors is the mapping of the Group dimension (different Q heads within a KV head group): If it is (at least partially) assigned to different cores (**spatial group allocation**), data sharing among cores will be observed in LLC; if it is completely mapped to the temporal domain (**temporal group allocation**), there will be no data sharing among cores, resembling conventional multi-head attention. To study its impact, in the following experiments, we allocate Group in Gemma3-27B completely to the temporal domain, while allowing that of the others to be mapped spatially. As we find benchmarks using spatial group allocation share similar characteristics in execution time, for brevity, we primarily show the results for Qwen3-8B.

D. Efficacy of Anti-thrashing Policy

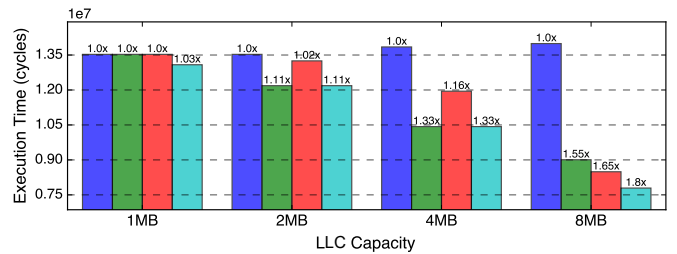
1) An intuitive view from a cache hit rate perspective:

Figure 3 illustrates the hit rate profile for a 4MB LLC. When thrashing occurs, LRU may exhibit a persistently low hit rate as useful blocks are continuously evicted under long reuse distance. In contrast, the at policy (anti-thrashing) aims to increase the hit rate by keeping a fixed set of data in the cache, based on the tag-bit scoring. The figure shows that at can achieve a consistently higher hit rate compared to LRU, particularly during phases of intense memory access.

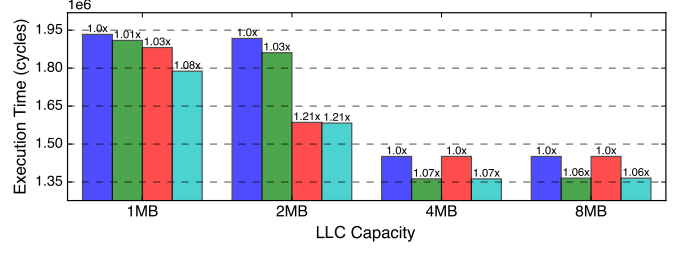
2) Comparison between anti-thrashing and LRU: Figure 4 presents the execution time (lower is better) of lru and at



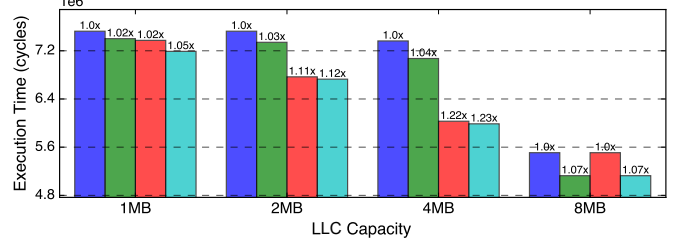
(a) Gemma3-27B, temporal group allocation, 2K sequence length



(b) Gemma3-27B, temporal group allocation, 4K sequence length



(c) Qwen3-8B, spatial group allocation, 2K sequence length



(d) Qwen3-8B, spatial group allocation, 4K sequence length

Fig. 4. Execution time for different LLC replacement policies and capacities. at: anti-thrashing. Unless otherwise specified, bypass for spatial group allocation cases refers to the gqa_bypass variant.

across various LLC capacities in Gemma and Qwen cases. The figure also includes an evaluation of bypassing strategies for a broader context, though the bypassing mechanism is discussed separately in Section VI-E. With moderate LLC capacities (2MB and 4MB), at consistently outperforms the standard LRU approach. With a 4MB LLC, such strategy achieves a 1.51x speedup in the Gemma 2K case and a 1.22x speedup in Qwen 4K. Similar improvements are observed with a 2MB LLC, indicating that the scoring mechanism effectively prioritizes specific cache lines, thereby reducing cache thrashing.

When the LLC capacity is much smaller than the working set, such as 1MB, the performance of both policies degrades significantly due to severe thrashing. However, the anti-thrashing policy still manages to provide a modest 1.08x

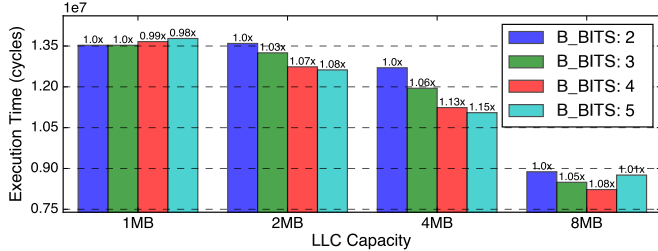


Fig. 5. Execution time for different anti-thrashing configurations (B_BITS) and capacities. Lower values indicate better performance (Gemma3-27B, 4K sequence length, temporal group allocation).

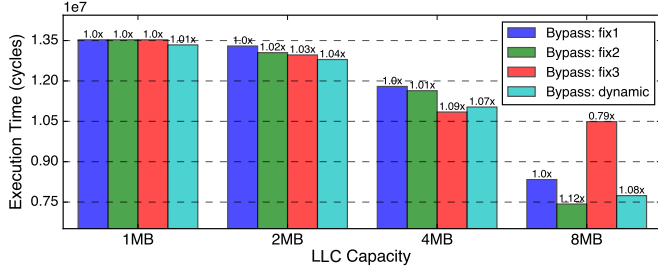


Fig. 6. Execution time for different cache bypass policies (Gemma3-27B, 4K sequence length, temporal group allocation), normalized against fix1. at is always enabled to show the additional benefits of bypassing.

speedup over LRU in the Gemma case and 1.02x in Qwen. This suggests that while the scoring mechanism can help mitigate some thrashing, its effectiveness is still limited under extremely constrained conditions.

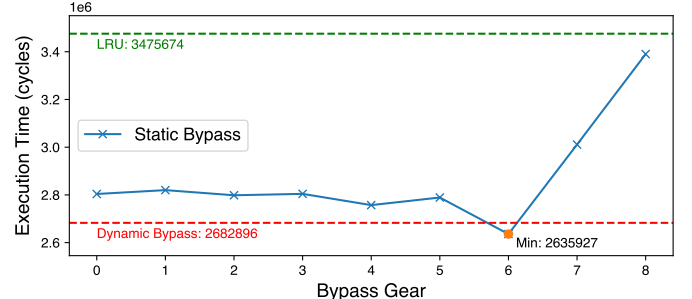
As the LLC capacity increases to 8MB, which is exactly the size of the active working set of the Gemma3-27B 2K case, both policies perform similarly with negligible differences. This is expected as LLC can now hold the entire working set, so the impact of replacement policies is minimized.

3) *Design choices of anti-thrashing policy:* A critical design parameter for the anti-thrashing policy is the number of tag bits used for scoring (B_BITS). In the evaluated setting, 3 bits are used, implying 8 distinct priority levels for cache lines. The choice of the number of bits involves a trade-off:

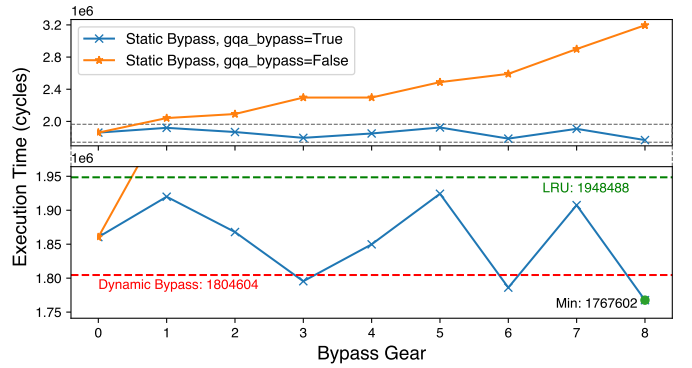
- **More bits** (e.g., 3-4 bits, yielding 8-16 levels) allows for a finer-grained classification of cache lines, which is particularly advantageous for moderately sized caches. It enables more nuanced prioritization without excessively restricting the working set available to the underlying LRU component, which manages lines with the same TMU score. However, if the cache is large enough that simple LRU already performs well, the overhead of managing many fine-grained levels might not provide additional benefits, or could even slightly degrade performance if the tag-bit heuristics are not perfectly aligned with actual data reuse patterns.

- **Fewer bits** (e.g., 1-2 bits, yielding 2-4 levels) results in a coarser classification. It is an effective strategy for aggressive anti-thrashing policy in very small or highly contended caches, as it partitions data into fewer distinct priority groups. However, for larger caches where thrashing is less of an issue, its restrictive nature could make the policy degenerate towards standard LRU, resulting in the premature eviction of useful data.

The optimal number of bits is likely application-specific and



(a) Gemma3-27B, temporal group allocation, 2K, 2MB LLC



(b) Qwen3-8B, spatial group allocation, 2K, 1MB LLC

Fig. 7. Execution time of static and dynamic bypassing with varying B_GEAR values. In both cases, B_BITS = 3, so $0 \leq B_GEAR \leq 8$. at is always enabled, so $B_GEAR = 0$ degenerates to ordinary at.

correlated with the cache size, associativity, and typical data access patterns. Our selection of 3 bits strikes a balance, providing distinct priority levels without excessive complexity. Figure 5 illustrates the performance with varying B_BITS and cache sizes. While there is no definitive optimal configuration across all scenarios, three bits consistently demonstrate stable speedup across different settings.

E. Efficacy of Dynamic Cache Bypassing

Since at already produces a stable improvement under both types of dataflows, here we focus on the **additional** effects of bypassing by always enabling anti-thrashing. We first compare our dynamic bypassing policy against several static ones with fixed bypassing gears (B_GEAR) to show its flexibility and near-optimality, followed by some discussions on its performance under different dataflows. Finally we compare bypassing with anti-thrashing to better understand their own advantageous regions and how they can collaborate to offer a higher speedup.

1) *Comparison between dynamic and static bypassing:* We first compare our dynamic bypass policy against three static ones, referred to as fix1, fix2, and fix3, which employ fixed B_GEARs in an ascending order. Figure 6 presents the execution times for each policy across LLC capacities from 1MB to 8MB.

The results highlight the fundamental drawback of static approaches: no single policy is optimal across all scenarios. The fix3 policy, the most aggressive among them, performs the best when the cache is highly contended. However, this same aggressiveness becomes detrimental as cache capacity

increases, making it the worst-performing policy at 8MB. Conversely, a less aggressive policy is more suitable for larger caches but is suboptimal under high contention.

Our dynamic policy overcomes this limitation by adapting its strategy under the guidance of eviction rate. It achieves the shortest execution time for 1MB and 2MB capacities and delivers performance close to the best static policy (*fix3*) at 4MB. Figure 7 further dives into 2 specific settings, one for each dataflow, and compares our dynamic policy with static ones of all possible gears. Under both dataflows, our policy can achieve near-optimality (within 3% difference), thereby demonstrating its robustness.

2) *Bypassing under different dataflows*: As explained in Section IV-E, bypassing can miss some inter-core reuse opportunities. The *gqa_bypass* variant is thus designed for such cases. Unless otherwise specified, *bypass* used in spatial group allocation dataflows throughout all the experiments refer to this variant. Figure 7(b) also includes an ablation study to showcase its efficacy. Without *gqa_bypass*, the performance of static bypassing (orange line) quickly degrades below LRU: the more it bypasses, the lower the performance. The only exception is at *B_GEAR* = 0, which means “to bypass nothing” and degenerates to the ordinary anti-thrashing policy (remember *at* is always enabled in this subsection). A dynamic bypassing policy under this circumstance will finally find its performance within the range of the orange line, which is still not likely to be better than LRU. However when *gqa_bypass* is enabled, bypassing can outperform LRU (blue line and red dashed line), despite the modest amount.

3) *Connection between bypassing and anti-thrashing*: After analyzing the properties of our bypassing policy, here we discuss how bypassing interacts with anti-thrashing. In Figure 4(a) and (b), *lru+bypass* yields more speedups than *at*, because the former can make use of the whole cache to pin data, while *at* has to set aside at least one cache line per set to temporarily store the victims. But in (c) and (d), the trend may differ since inter-core reuse exists and we have to adopt the more conservative *gqa_bypass* variant. However, in all these cases, combining *at* and *bypass* does produce the best speedups. This is because anti-thrashing can further filter out over-sized working sets when bypassing alone is not precise enough, for example, when it is still under dynamic adaption. It is also worth noting that when cache sizes are sufficient, bypassing can still bring additional speedups, e.g., a 1.07x speedup in Figure 4(d) 8MB. This is because bypassing in this case reduces the cache bandwidth pressure and makes use of the idle DRAM bandwidth.

F. Efficacy of Dead Block Prediction

DBP is designed to enhance cache efficiency by proactively identifying and evicting data that is no longer needed. Its effectiveness is particularly pronounced in workloads with distinct temporal phases, such as when multiple KV heads are mapped to the temporal domain, and in the multi-batch inference scenario evaluated here. In this context, data from completed batches becomes “dead” and pollutes the cache, contending for resources with active data from the current

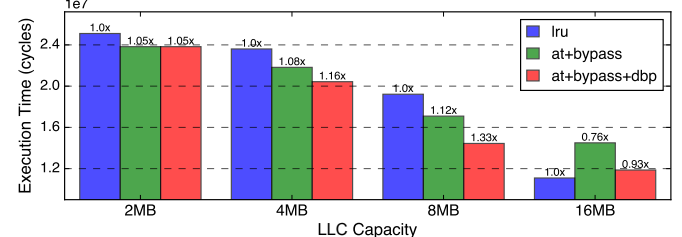


Fig. 8. Performance impact of DBP in a multi-batch scenario (Gemma3-27B, 4K sequence length, 2 batches). The chart compares execution time for *at+bypass* (anti-thrashing and bypassing) against the one which adds DBP.

batch. To precisely quantify the benefits of DBP, we compare the performance of the DBP strategy—in cooperation with the anti-thrashing and bypassing mechanisms—against the standard *at+bypass* policy.

The results in Figure 8 show that DBP offers significantly better performance, particularly when the cache is moderately sized. With a 4MB LLC, the addition of DBP provides a **1.07x** speedup. Similarly, for an 8MB LLC, DBP provides a strong **1.19x** speedup. In these settings, the cache is aggressively contended for data from the current and previous batches. However, the standard *at* policy cannot directly distinguish useful data from the current batch and obsolete data from previous batches. DBP resolves this ambiguity by identifying the prior batches’ data as dead, allowing the replacement policy to efficiently clear useless data.

Things are different when the cache size is extremely constrained, such as 2MB, which is much smaller than the working set size. Here, the cache is so small that *at* already evicts out most of the incoming lines, including those dead, which explains the marginal improvement brought by DBP (1.01x). However, this is a special case; under normal circumstances, dead blocks must still be explicitly distinguished to provide accurate information for cache replacement.

Another scenario is that, LRU provides the best performance at 16MB, where the entire working set fits into the cache. In this case, there is no cache contention, and all data can be accommodated without eviction. LRU is able to switch to another working set due to its nature of retaining recently used data, and the overhead of DBP in tracking dead blocks becomes unnecessary. Policy *at*, however, performs the worst in this case, as it is not able to utilize the full cache space effectively due to cache pollution.

In conclusion, DBP is particularly powerful for workloads with periodical data retirement under moderately sized caches. It works in harmony with other cache management strategies so that they can filter out the data to be held in the cache using their own criteria without interference from dead blocks.

G. Evaluation on Longer Contexts via Analytical Model

Real-world LLMs and long-context scenarios can be computationally prohibitive for cycle-level simulation. To verify the effectiveness of our design in such cases, we turn to the analytical model in Section V. We restate that the model is intended to fit the performance for several key variants of our policies instead of every possible configuration.

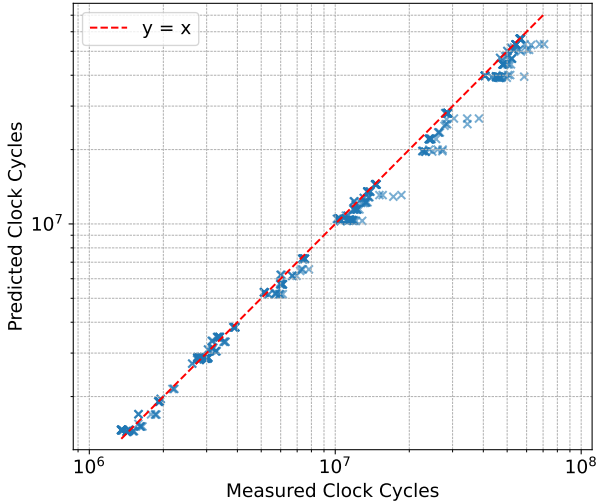


Fig. 9. Comparison between simulation and analytical model results

1) *Validating the analytical model*: We perform validation across the following design and mapping space:

- LLC size: 1MB, 2MB, 4MB
- policies: lru, dbp, at+dbp, bypass+dbp, all
- bypass variants: fix1, fix3, optimal
- gqa_bypass: true if spatial group allocation else false
- workloads: Gemma3-27B, Llama3-70B, Qwen3-8B
- sequence length: 2K, 4K, 8K
- dataflow: {spatial/temporal} group allocation

In the listing above, `all=at+bypass+dbp`; we always enable `dbp` except for `lru` since it provides a clean separation between adjacent working sets, making it easier for `at` and `bypass` to perform well. `optimal` is a static bypassing variant with optimal B_GEAR, which is theoretically the upper limit of our final dynamic bypassing policy. We use it as a delegate since we have empirically confirmed the near-optimality of our dynamic policy in Section VI-E. As for the dataflow, we always map the Group dimension in the temporal domain inside other embarrassingly parallel dimensions such as batch, K/V heads, and the sequence length of the Q tensor. We do not include other design space parameters like the number of cores, SIMD lanes, and LSUs in this section for the following reasons: (1) We are extending the measurement results for the same hardware setting as in previous sections; (2) Changing the cache size is already sufficient to sweep through the spectrum from compute-bound to memory-bound cases. A total of 486 data points ($= 3$ (cache_size) $\times 3$ (seq_len) $\times 6$ (workload & dataflow) $\times 12$ (policies: 3 (lru, dbp, at+dbp) + 3 (bypass variant) $\times 3$ (bypass+dbp, all)) have been extracted from the design space, of which the simulated and predicted execution time are shown in Figure 9. We deem this scale to be sufficient since the execution time has spanned almost 2 orders of magnitude. The fitting result shows a correlation coefficient of $R^2 = 0.997$ and a Kendall $\tau = 0.934$, which shows that our model provides sufficient accuracy and preserves order to a large extent.

2) *Evaluating larger workloads*: The workloads include Gemma3-27B, Llama3-70B, Llama3-405B, and Qwen3-8B, with sequence lengths extending to 64K, 128K, and 256K. To align with previous sections, here we also apply temporal

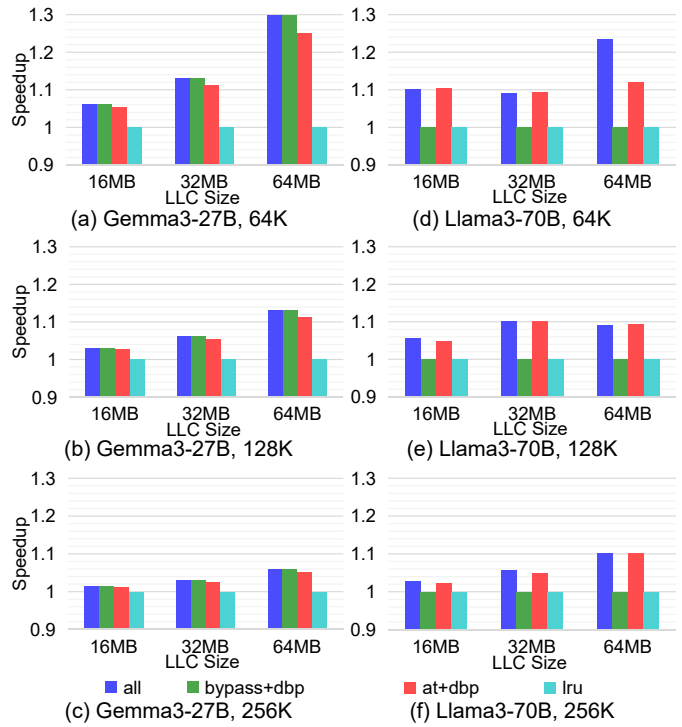


Fig. 10. Speedups (normalized to LRU) of the proposed cache orchestration strategies under longer sequence lengths, evaluated with the analytical model.

group allocation to Gemma3 and spatial to other cases. The LLC size is swept across 16MB, 32MB, and 64MB.

Figure 10 illustrates the speedup of different configurations: the full DCO design (`all`), optimal bypassing with dead block prediction (`bypass+dbp`), anti-thrashing with dead block prediction (`at+dbp`), and baseline LRU.

Baseline Analysis (LRU): We find that the absolute execution time for LRU maintains almost identical across 16MB, 32MB, and 64MB caches. This is because the working set size is far beyond the LLC size, leading to severe thrashing and a very low hit rate that is irrelevant to the cache size. All speedups reported in Figure 10 are normalized to this baseline.

Performance on Gemma3: For Gemma3-27B (a)-(c), our proposed DCO design achieves significant speedups, peaking at approximately 1.30 \times with a 64MB cache. We observe that the efficacy of the combined strategy scales positively with cache size. Similar to previous simulation results, we also see `bypass+dbp` outperforms `at+dbp` since the latter cannot use the whole cache to pin data. However, adding `at` to `bypass+dbp` (`all`) here only makes marginal difference. This is because we are assuming `optimal` bypassing and neglecting non-ideal factors in dynamic bypassing such as the period of dynamic adaption.

Performance on Llama3 and Generalization: The results for Llama3-70B (d)-(f) exhibit a different characteristic. Here, `bypass+dbp` yields negligible improvement (speedup ≈ 1.0), indicating that the `gqa_bypass` variant **alone** struggles to improve over LRU under cases with inter-core reuse. `at+dbp`, as expected, remains highly effective and contributes to the majority of the performance gains (up to 1.12 \times). The full design (`all`) successfully integrates these features to maximize speedup.

We further validated Llama3-405B and Qwen3-8B using the same methodology. We found that their performance trends and sensitivity to cache management strategies are similar to those of Llama3-70B shown in Figure 10(d)-(f). This indicates that for these dense, long-context models, identifying dead blocks and protecting the working set via anti-thrashing are the dominant factors for improving performance.

VII. RELATED WORK

Previous research on optimizing multi-core GPUs and AI accelerators can be broadly categorized into two areas: optimizing chips with global on-chip buffers and optimizing chips without them. Furthermore, many well-known studies focus on cache management across different architectures, including CPUs, GPUs, and certain embedded processors. Our research significantly diverges from these studies, particularly concerning the target architecture and workloads.

A. Global Buffer Management in Multi-core AI Accelerators

The efficient utilization of the global on-chip buffer has been studied by several research papers. Approaches like Pin-or-Fuse [15] and OnSRAM [32] have been proposed to enhance on-chip data reuse, which minimizes off-chip data transfer. These methods are fundamentally software compilation optimizations. However, as Telamalloc [30] emphasizes, memory buffer allocation is a crucial step in launching applications for specific scenarios. Consequently, these additional management passes can slow down the compilation process. In contrast, our method with a global cache doesn't require complex buffer management and substantially reduces compilation efforts.

B. Optimizing Multi-core AI Accelerators without a Global Buffer

Not all works from the academia include a global buffer in their design. For example, Tangram [12] and Atomic Dataflow [44] do not rely on a global on-chip buffer, unlike many dataflow and architectural improvements. These systems might instead create specific on-chip data transfer routes to facilitate data reuse.

Although these designs might lower resource usage on chips, they are often tailored to specific applications, primarily convolutional neural networks (CNN). According to the Google TPUv4 report [17], as of October 2022, 57% of TPUs were employed for Transformer training, whereas only 12% were used for CNN, highlighting the restricted influence of these designs.

Using a shared SRAM buffer will effectively reduce the bandwidth gap between private buffers and DRAMs. Additionally, accelerators with shared memory, in contrast to buffer-free designs, do not rely on any assumptions about the graph-level structure of the workload, making them suitable for a broader array of applications and deserving of increased focus.

C. Cache Management and Bypass

Our cache management strategy consists of two aspects: dead block prediction and bypassing. Various strategies [1],

[14], [16], [22], [23], [25], [26], [29], [38], [41] have been developed to forecast inactive cache blocks in CPU caches, enabling timely dead block clearance or bypassing the last access. These methods aim to increase prediction accuracy and reduce hardware costs using techniques like sampling- and counter-based methods. In contrast to general-purpose scenarios, our focus is on application-specific platforms, which provide detailed insights into memory access patterns and avoid the necessity for general-purpose techniques. We adopt the sampling concept from earlier studies to minimize hardware expenses.

Cache bypassing is an effective strategy to mitigate resource contention and enhance application performance. Recent advancements emphasize the utilization of learning-based methods to optimize cache bypassing. RLR [35] employs reinforcement learning (RL) as an offline tool for designing efficient cache replacement and bypassing policies. However, their focus is on the CPU, which differs from our primary concern. The work in [43] introduces the concept of dynamic cache bypassing, which is insightful for our design. It employs an online learning mechanism to determine, on-the-fly, the optimal proportion of thread blocks that should bypass the cache for these “medium locality” accesses. However, it only targets GPUs and does not explore the coordination between bypassing and cache replacement policy, which is a unique perspective that our work features.

D. AI accelerator analytical models

Analytical models are valuable for design space exploration (DSE) and verifying early-stage designs, offering rapid insights into performance and power usage. Timeloop [33] is a flexible modeling platform for DNN accelerators, delivering performance and energy estimation to evaluate trade-offs. Stream [39] facilitates layer fusion and supports various multi-core architectures for comprehensive DSE. The Neural Network Dataflow Scheduling tool [11], [12] allows for energy-efficient dataflow and mapping exploration, utilizing a tiled multi-core architecture where each core mimics an Eyeriss-style [5] engine. FRAME [20] uses a roofline model to assess different operators across various NNs, providing insights into the compute/memory ratio in accelerator design. Nonetheless, these models often exclude caches in hardware setups. Our cache-integrated model opens up new possibilities for DSE.

VIII. CONCLUSION

In this work, we introduce DCO, a hybrid architecture that optimizes data reuse in multi-core AI systems equipped with a shared cache. Experiments show that the three measures, dead block prediction, anti-thrashing, and bypassing have their own advantageous ranges and can be combined to offer better results (up to 1.8x speedup). We have also built and validated an analytical model that considers realistic overlapping behaviors to evaluate our design under practical and larger workloads. Evaluation via this model further confirms our strategies outperform conventional LRU caches under longer sequence lengths, though moderate cache sizes are still preferred: when the LLC is too small, all policies suffer from severe thrashing;

when it is too large to hold the full working set (a large LLC also leads to a significant hardware cost), the choice of replacement/bypass policy becomes largely irrelevant.

REFERENCES

- [1] J. Abella, A. González, X. Vera, and M. F. P. O’Boyle, “Iatac: A smart predictor to turn-off l2 cache lines,” *ACM Trans. Archit. Code Optim.*, vol. 2, no. 1, p. 55–77, mar 2005. [Online]. Available: <https://doi.org/10.1145/1061267.1061271>
- [2] J. Bachrach, H. Vo, B. Richards, Y. Lee, A. Waterman, R. Avižienis, J. Wawrzynek, and K. Asanović, “Chisel: constructing hardware in a scala embedded language,” in *Proceedings of the 49th Annual Design Automation Conference*, ser. DAC ’12. New York, NY, USA: Association for Computing Machinery, 2012, p. 1216–1225. [Online]. Available: <https://doi.org/10.1145/2228360.2228584>
- [3] M. Brehob and R. Enbody, “An analytical model of locality and caching,” Michigan State University, Department of Computer Science and Engineering, Tech. Rep. MSU-CSE-99-31, 1999.
- [4] cambricon Corporation. (2024) Bang c ops develop-guide. [Online]. Available: <https://github.com/Cambricon/mlu-ops/blob/master/docs/BANG-C-OPS-Develop-Guide.md>
- [5] Y.-H. Chen, J. Emer, and V. Sze, “Eyeriss: A spatial architecture for energy-efficient dataflow for convolutional neural networks,” in *Proceedings of the 43rd International Symposium on Computer Architecture*, ser. ISCA ’16. IEEE Press, 2016, p. 367–379. [Online]. Available: <https://doi.org/10.1109/ISCA.2016.40>
- [6] Q. Corporation. (2023) Snapdragon x elite. [Online]. Available: <https://www.qualcomm.com/snapdragon/laptops>
- [7] P. Cronin, X. Gao, H. Wang, and C. Cotton, “An exploration of arm system-level cache and gpu side channels,” in *Proceedings of the 37th Annual Computer Security Applications Conference*, ser. ACSAC ’21. New York, NY, USA: Association for Computing Machinery, 2021, p. 784–795. [Online]. Available: <https://doi.org/10.1145/3485832.3485902>
- [8] T. Dao, “Flashattention-2: Faster attention with better parallelism and work partitioning,” 2023. [Online]. Available: <https://arxiv.org/abs/2307.08691>
- [9] T. Dao, D. Y. Fu, S. Ermon, A. Rudra, and C. Ré, “Flashattention: Fast and memory-efficient exact attention with io-awareness,” 2022. [Online]. Available: <https://arxiv.org/abs/2205.14135>
- [10] J. Fang, Z.-Y. Leng, S.-T. Liu, Z.-C. Yao, and X.-F. Sui, “Exploring heterogeneous noc design space in heterogeneous gpu-cpu architectures,” *Journal of Computer Science and Technology*, vol. 30, no. 1, pp. 74–83, 2015.
- [11] M. Gao, J. Pu, X. Yang, M. Horowitz, and C. Kozyrakis, “Tetris: Scalable and efficient neural network acceleration with 3d memory,” *SIGARCH Comput. Archit. News*, vol. 45, no. 1, p. 751–764, apr 2017. [Online]. Available: <https://doi.org/10.1145/3093337.3037702>
- [12] M. Gao, X. Yang, J. Pu, M. Horowitz, and C. Kozyrakis, “Tangram: Optimized coarse-grained dataflow for scalable nn accelerators,” in *Proceedings of the Twenty-Fourth International Conference on Architectural Support for Programming Languages and Operating Systems*, ser. ASPLOS ’19. New York, NY, USA: Association for Computing Machinery, 2019, p. 807–820. [Online]. Available: <https://doi.org/10.1145/3297858.3304014>
- [13] H. Genc, A. Haj-Ali, V. Iyer, A. Amid, H. Mao, J. Wright, C. Schmidt, J. Zhao, A. Ou, M. Banister *et al.*, “Gemmini: An agile systolic array generator enabling systematic evaluations of deep-learning architectures,” *arXiv preprint arXiv:1911.09925*, vol. 3, p. 25, 2019.
- [14] Z. Hu, S. Kaxiras, and M. Martonosi, “Timekeeping in the memory system: predicting and optimizing memory behavior,” in *Proceedings 29th Annual International Symposium on Computer Architecture*, 2002, pp. 209–220.
- [15] H.-J. Jeong, J. Yeo, C. Bahk, and J. Park, “Pin or fuse? exploiting scratchpad memory to reduce off-chip data transfer in dnn accelerators,” in *Proceedings of the 21st ACM/IEEE International Symposium on Code Generation and Optimization*, ser. CGO 2023. New York, NY, USA: Association for Computing Machinery, 2023, p. 224–235. [Online]. Available: <https://doi.org/10.1145/3579990.3580017>
- [16] D. A. Jiménez and E. Teran, “Multiperspective reuse prediction,” in *Proceedings of the 50th Annual IEEE/ACM International Symposium on Microarchitecture*, ser. MICRO-50 ’17. New York, NY, USA: Association for Computing Machinery, 2017, p. 436–448. [Online]. Available: <https://doi.org/10.1145/3123939.3123942>
- [17] N. P. Jouppi, G. Kurian, S. Li, P. Ma, R. Nagarajan, L. Nai, N. Patil, S. Subramanian, A. Swing, B. Towles, C. Young, X. Zhou, Z. Zhou, and D. Patterson, “Tpu v4: An optically reconfigurable supercomputer for machine learning with hardware support for embeddings,” 2023.
- [18] N. P. Jouppi, C. Young, N. Patil, D. Patterson, G. Agrawal, R. Bajwa, S. Bates, S. Bhatia, N. Boden, A. Borchers *et al.*, “In-datacenter performance analysis of a tensor processing unit,” in *Proceedings of the 44th annual international symposium on computer architecture*, 2017, pp. 1–12.
- [19] S.-C. Kao, S. Subramanian, G. Agrawal, A. Yazdanbakhsh, and T. Krishna, “Flat: An optimized dataflow for mitigating attention bottlenecks,” in *Proceedings of the 28th ACM International Conference on Architectural Support for Programming Languages and Operating Systems, Volume 2*, ser. ASPLOS 2023. New York, NY, USA: Association for Computing Machinery, 2023, p. 295–310. [Online]. Available: <https://doi.org/10.1145/3575693.3575747>
- [20] S.-C. Kao, S. Subramanian, A. Bambhaniya, and T. Krishna, “FRAME: Fast Roofline Analytical Modeling and Estimation,” 2022. [Online]. Available: <https://github.com/maestro-project/frame>
- [21] M. Khairy, Z. Shen, T. M. Aamodt, and T. G. Rogers, “Accel-sim: An extensible simulation framework for validated gpu modeling,” in *2020 ACM/IEEE 47th Annual International Symposium on Computer Architecture (ISCA)*. IEEE, 2020, pp. 473–486.
- [22] S. M. Khan, Y. Tian, and D. A. Jiménez, “Sampling dead block prediction for last-level caches,” in *2010 43rd Annual IEEE/ACM International Symposium on Microarchitecture*, 2010, pp. 175–186.
- [23] M. Kharbutli and Y. Solihin, “Counter-based cache replacement and bypassing algorithms,” *IEEE Transactions on Computers*, vol. 57, no. 4, pp. 433–447, 2008.
- [24] S. Kim, C. Hooper, T. Wattanawong, M. Kang, R. Yan, H. Genc, G. Dinh, Q. Huang, K. Keutzer, M. W. Mahoney *et al.*, “Full stack optimization of transformer inference: a survey,” *arXiv preprint arXiv:2302.14017*, 2023.
- [25] A.-C. Lai and B. Falsafi, “Selective, accurate, and timely self-validation using last-touch prediction,” in *Proceedings of 27th International Symposium on Computer Architecture (IEEE Cat. No.RS00201)*, 2000, pp. 139–148.
- [26] A.-C. Lai, C. Fide, and B. Falsafi, “Dead-block prediction & dead-block correlating prefetchers,” in *Proceedings 28th Annual International Symposium on Computer Architecture*, 2001, pp. 144–154.
- [27] C. Lai, Z. Zhou, A. Poptani, and W. Zhang, “Lcm: Llm-focused hybrid spm-cache architecture with cache management for multi-core ai accelerators,” in *Proceedings of the 38th ACM International Conference on Supercomputing*, ser. ICS ’24. New York, NY, USA: Association for Computing Machinery, 2024, p. 62–73. [Online]. Available: <https://doi.org/10.1145/3650200.3656592>
- [28] H. Liao, J. Tu, J. Xia, and X. Zhou, “Davinci: A scalable architecture for neural network computing,” in *Hot Chips Symposium*, 2019, pp. 1–44.
- [29] H. Liu, M. Ferdman, J. Huh, and D. Burger, “Cache bursts: A new approach for eliminating dead blocks and increasing cache efficiency,” in *2008 41st IEEE/ACM International Symposium on Microarchitecture*, 2008, pp. 222–233.
- [30] M. Maas, U. Beaugnon, A. Chauhan, and B. Ilbeyi, “Telamalloc: Efficient on-chip memory allocation for production machine learning accelerators,” in *Proceedings of the 28th ACM International Conference on Architectural Support for Programming Languages and Operating Systems, Volume 1*, ser. ASPLOS 2023. New York, NY, USA: Association for Computing Machinery, 2022, p. 123–137. [Online]. Available: <https://doi.org/10.1145/3567955.3567961>
- [31] M. Martins, J. M. Matos, R. P. Ribas, A. Reis, G. Schlinker, L. Rech, and J. Michelsen, “Open cell library in 15nm freepdk technology,” in *Proceedings of the 2015 Symposium on International Symposium on Physical Design*, ser. ISPD ’15. New York, NY, USA: Association for Computing Machinery, 2015, p. 171–178. [Online]. Available: <https://doi.org/10.1145/2717764.2717783>
- [32] S. Pal, S. Venkataramani, V. Srinivasan, and K. Gopalakrishnan, “Onram: Efficient inter-node on-chip scratchpad management in deep learning accelerators,” *ACM Trans. Embed. Comput. Syst.*, vol. 21, no. 6, oct 2022. [Online]. Available: <https://doi.org/10.1145/3530909>
- [33] A. Parashar, P. Raina, Y. S. Shao, Y.-H. Chen, V. A. Ying, A. Mukkara, R. Venkatesan, B. Khailany, S. W. Keckler, and J. Emer, “Timeloop: A systematic approach to dnn accelerator evaluation,” in *2019 IEEE International Symposium on Performance Analysis of Systems and Software (ISPASS)*, 2019, pp. 304–315.
- [34] A. Reuther, P. Michaleas, M. Jones, V. Gadepally, S. Samsi, and J. Kepner, “Ai accelerator survey and trends,” in *2021 IEEE High*

Performance Extreme Computing Conference (HPEC). IEEE, 2021, pp. 1–9.

[35] S. Sethumurugan, J. Yin, and J. Sartori, “Designing a cost-effective cache replacement policy using machine learning,” in *2021 IEEE International Symposium on High-Performance Computer Architecture (HPCA)*, 2021, pp. 291–303.

[36] J. Shah, G. Bikshandi, Y. Zhang, V. Thakkar, P. Ramani, and T. Dao, “Flashattention-3: Fast and accurate attention with asynchrony and low-precision,” 2024. [Online]. Available: <https://arxiv.org/abs/2407.08608>

[37] Y. S. Shao, J. Cemons, R. Venkatesan, B. Zimmer, M. Fojtik, N. Jiang, B. Keller, A. Klinefelter, N. Pinckney, P. Raina, S. G. Tell, Y. Zhang, W. J. Dally, J. Emer, C. T. Gray, B. Khailany, and S. W. Keckler, “Simba: Scaling deep-learning inference with chiplet-based architecture,” *Commun. ACM*, vol. 64, no. 6, p. 107–116, may 2021. [Online]. Available: <https://doi.org/10.1145/3460227>

[38] S. Somogyi, T. F. Wenisch, N. Hardavellas, J. Kim, A. Ailamaki, and B. Falsafi, “Memory coherence activity prediction in commercial workloads,” in *Proceedings of the 3rd Workshop on Memory Performance Issues: In Conjunction with the 31st International Symposium on Computer Architecture*, ser. WMPI ’04. New York, NY, USA: Association for Computing Machinery, 2004, p. 37–45. [Online]. Available: <https://doi.org/10.1145/1054943.1054949>

[39] A. Symons, L. Mei, S. Colleman, P. Houshmand, S. Karl, and M. Verhelst, “Stream: A modeling framework for fine-grained layer fusion on multi-core dnn accelerators,” in *2023 IEEE International Symposium on Performance Analysis of Systems and Software (ISPASS)*, 2023, pp. 355–357.

[40] S. Van den Steen, S. Eyerman, S. De Pestel, M. Mechri, T. E. Carlson, D. Black-Schaffer, E. Hagersten, and L. Eeckhout, “Analytical processor performance and power modeling using micro-architecture independent characteristics,” *IEEE Transactions on Computers*, vol. 65, no. 12, pp. 3537–3551, 2016.

[41] C.-J. Wu, A. Jaleel, W. Hasenplauth, M. Martonosi, S. C. Steely, and J. Emer, “Ship: Signature-based hit predictor for high performance caching,” in *Proceedings of the 44th Annual IEEE/ACM International Symposium on Microarchitecture*, ser. MICRO-44. New York, NY, USA: Association for Computing Machinery, 2011, p. 430–441. [Online]. Available: <https://doi.org/10.1145/2155620.2155671>

[42] S. Xi, Y. Yao, K. Bhardwaj, P. Whatmough, G.-Y. Wei, and D. Brooks, “Smaug: End-to-end full-stack simulation infrastructure for deep learning workloads,” *ACM Transactions on Architecture and Code Optimization (TACO)*, vol. 17, no. 4, pp. 1–26, 2020.

[43] X. Xie, Y. Liang, Y. Wang, G. Sun, and T. Wang, “Coordinated static and dynamic cache bypassing for gpus,” in *2015 IEEE 21st International Symposium on High Performance Computer Architecture (HPCA)*, 2015, pp. 76–88.

[44] S. Zheng, X. Zhang, L. Liu, S. Wei, and S. Yin, “Atomic dataflow based graph-level workload orchestration for scalable dnn accelerators,” in *2022 IEEE International Symposium on High-Performance Computer Architecture (HPCA)*, 2022, pp. 475–489.

[45] Z. Zhou, C. Lai, and W. Zhang, “Llamcat: Optimizing large language model inference with cache arbitration and throttling,” 2025, to appear in the Proceedings of the 54th International Conference on Parallel Processing (ICPP 2025). [Online]. Available: <https://arxiv.org/abs/2512.00083>

IX. BIOGRAPHY SECTION



Zhongchun Zhou received the B.E. degree in microelectronic engineering from the School of Integrated Circuits, Tsinghua University, Beijing, China, in 2022. He is currently pursuing the Ph.D. degree in electronic and computer engineering with the Hong Kong University of Science and Technology, Hong Kong. His research interests include integrated circuits, field-programmable gate arrays (FPGAs), high performance computing (HPC) and computer architecture, with a focus on hardware acceleration and system optimization for large language models.



Chengtao Lai received the B.E. degree in Engineering Mechanics from the School of Aerospace Engineering, Tsinghua University, Beijing, China, in 2021. He is currently pursuing the Ph.D. degree in Electronic and Computer Engineering with the Hong Kong University of Science and Technology, Hong Kong. His research interests include high performance computing and computer architecture, especially the memory subsystem of AI accelerators.



Yuhang Gu is currently an undergraduate student from the School of Electronic Science and Engineering, Southeast University, Nanjing, China, since 2022. He is interested in research on computer systems, advanced computing systems including high performance computing and quantum computing, integrated circuits and computer architecture.



Wei Zhang (Fellow, IEEE) received the Ph.D. degree from Princeton University, Princeton, NJ, USA, in 2009. She was an Assistant Professor with the School of Computer Engineering, Nanyang Technological University, Singapore, from 2010 to 2013. She joined the Hong Kong University of Science and Technology, Hong Kong, in 2013, where she is currently a Professor and she established the Reconfigurable Computing System Laboratory. She has authored or coauthored over 80 book chapters and papers in peer-reviewed journals and international conferences. Her current research interests include reconfigurable systems, FPGA-based design, low-power high-performance multicore systems, electronic design automation, embedded systems, and emerging technologies. Dr. Zhang serves as an Associate Editor for ACM Transactions on Embedded Computing Systems, IEEE Transactions on Very Large Scale Integration (VLSI) Systems, and ACM Journal of Emerging Technologies in Computing Systems. She also serves on many organization committees and technical program committees.